Journal of Materials Chemistry A

Encapsulated C12A7 electride material enables multistep electron transfer process for cross-coupling reactions

Journal:	*Journal of Materials Chemistry A*
Manuscript ID	TA-ART-11-2022-008899.R1
Article Type:	Paper
Date Submitted by the Author:	12-Jan-2023
Complete List of Authors:	Dai, Bo; Shanghai Jiao Tong University Li, Zichuang; Shanghai Jiao Tong University Xu, Miao; Shanghai Institute of Space Power-Sources Li, Jiang; Tokyo Institute of Technology Lu, Yangfan; Chongqing University, Zai, Jiantao; Shanghai Jiao Tong University, Fan, Liuyin; Shanghai Jiao Tong University, School of Life Science and Biotechnology Park, Sang-Won; The University of Suwon Sasase, Masato ; Tokyo Institute of Technology, Materials Research Center for Element Strategy, Tokyo Institute of Technology Kitano, Masaaki; Tokyo Institute of Technology, Materials Research Center for Element Strategy Hosono,, Hideo; Tokyo Institute of Technology Li, Xin-Hao; Shanghai Jiao Tong University, Ye, Tian-Nan; Jiaotong University, Chen, Jie-Sheng; Shanghai Jiao Tong University,

SCHOLARONE™
Manuscripts

ARTICLE

Encapsulated C12A7 electride material enables multistep electron transfer process for cross-coupling reactions

Received 00th January 20xx,
Accepted 00th January 20xx

DOI: 10.1039/x0xx00000x

Bo Dai,[#a] Zichuang Li,[#a] Miao Xu,[#b] Jiang Li,[c] Yangfan Lu,[d] Jiantao Zai,[a] Liuyin Fan,[e] Sang-Won Park,[f] Masato Sasase,[c] Masaaki Kitano,[*c] Hideo Hosono,[*c] Xin-Hao Li,[a] Tian-Nan Ye,[*a] Jie-Sheng Chen[*a]

10th Anniversary Statement

We would like to congratulate on the upcoming 10th anniversary celebration of Journal of Materials Chemistry A. In the discipline of materials and chemistry, Journal of Materials Chemistry A has a great influence that cannot be ignored. Many excellent opinions and articles have been published here, playing a decisive role in the profession. As materials chemistry researchers, we feel honoured to publish articles in Journal of Materials Chemistry A. In the past ten years, measurable progress on the research of materials chemistry in which the future of energy and sustainability is embodied. Electride materials are regarded as one category of promising emergent materials that have more advantages than traditional catalytic materials because of their unique electronic properties which can accelerate or limit specific chemical reactions. At present, there are few cases in which electride materials are used in industrial catalysis because of its chemical instability. Our research goal is to solve this problem and to develop stable electride composite materials that can be successfully put into use in the near future through continuous technological breakthroughs.

The electronic structures of active sites fundamentally determine the catalytic performance in chemical reactions, and is also crucial to get detailed understanding of charge transport and reaction mechanism. In the current study, the regulation of the electronic structure of active metal Pd can be achieved through a multi-step electron transfer process formed by a synergy of $[Ca_{24}Al_{28}O_{64}]^{4+}(e^-)_4$ (C12A7:e$^-$) electride and conductive graphene (Gr). The composite catalytic system (Pd/Gr/C12A7:e$^-$) significantly facilitates the transfer of electrons from electron-rich Pd active sites to aryl halides in Suzuki-coupling reactions, which enables superior catalytic performance with above 20-times TOFs higher than well-studied negatively charged Pd catalysts. No catalytic degradation was observed even after impregnating the catalyst in water because of the well protected C12A7:e$^-$ electride by Gr. The present efficient catalyst can further trigger various carbon-carbon cross-coupling reactions with high activities. These results provide significant advantages for the expansion of the potential applications of electride materials, allowing precise control of the electronic structure of the active sites and thus aid in tuning the reaction conditions using a simple method.

1. Introduction

Cross coupling is of fundamental significance in the formation of carbon-carbon bond as well as an important class of reaction in organic synthesis.[1-4] It was initially investigated with homogeneous catalysts with electron-rich Pd active sites by the introduction of electron donating ligands that were designed to reduce the high energy barrier of the reactants associated with rate determining step and further enhance the catalytic activity.[5-7] However, the combination of unrecyclable Pd species and potentially toxic ligands, e.g., Pd-based phosphine complex has raised tremendous environmental concerns amid increasing demands for sustainability in the chemical industry.[8,9] As such, heterogeneous catalysts have a distinct advantage in their facile recyclability without employing ligand promoters.[10-15] While many studies on heterogeneous catalysts have been focused on the design of electron-rich Pd active sites by the introduction of

[a.] Frontiers Science Center for Transformative Molecules, School of Chemistry and Chemical Engineering, Shanghai Jiao Tong University, Shanghai 200240, China. E-mail: ytn2011@sjtu.edu.cn; chemcj@sjtu.edu.cn.
[b.] State Key Laboratory of Space Power-sources Technology, Shanghai Institute of Space Power-Sources, Shanghai 200245, China.
[c.] MDX Research Center for Element Strategy, International Research Frontiers Initiative, Tokyo Institute of Technology, 4259 Nagatsuta, Midori-ku, Yokohama 226-8503, Japan. E-mail: kitano.m.aa@m.titech.ac.jp; hosono@mces.titech.ac.jp.
[d.] National Engineering Research Center for Magnesium Alloys, College of Materials Science and Engineering, Chongqing University, Chongqing 400030, China.
[e.] Student Innovation Center, Shanghai Jiao Tong University, Shanghai 200240, China.
[f.] Department of Chemical and Materials Engineering, University of Suwon, Hwaseong, Gyeonggi 18323, Republic of Korea.
[#] These authors have contributed equally.
† Electronic Supplementary Information (ESI) available: See DOI: 10.1039/x0xx00000x

multi-metallic components or organic modifiers, the occupation of Pd sites by other elements always results in inferior catalytic activity. [16,17] Here, we focus on an approach that utilizes metal-support interactions, in which the electronic structure of the active metal can be effectively controlled by the support material that favour the enhancement of the catalytic activity.[18-23]

$[Ca_{24}Al_{28}O_{64}]^{4+}(e^-)_4$ (C12A7:e⁻) electride materials, which accommodate anionic electrons in their periodically distributed lattice, have been drawing considerable attention because their low work function feature enables strong electron donation ability.[24-30] One of their most successful applications is ammonia synthesis, in which an electron transfer from C12A7:e⁻ electride to the antibonding orbitals of N_2 facilitates N_2 dissociation and the overall activation energy of the reaction was suppressed.[31-34] However, C12A7:e⁻ electride is typically prepared by a solid-state method, resulting in a small surface area with a few square meters per gram. Such low surface area leads to a relative low dispersion of the loaded active metals and thus only exposure of limited active sites. Moreover, the moisture sensitivity of C12A7:e⁻ severely restricts further applications in aqueous reactions.[35,36] Therefore, it is highly desired to realize C12A7:e⁻ electride with high stability towards moisture while retaining its intrinsic electronic structure. Graphene (Gr)-based materials have been well-studied as water or gas filters,[37,38] and thus we are inspired to combine C12A7:e⁻ electride with Gr to form an encapsulated nano-structure.

Here we report the successful preparation of Pd/Gr/C12A7:e⁻ catalyst and its high catalytic activity towards cross-coupling reactions. In this composite material, C12A7:e⁻ electride surface was coated with Gr layers, which are highly dispersed with nanometric Pd clusters, to achieve high chemical stability towards moisture. Negatively charged Pd was realized through a multistep electron transfer process, in which electrons can be donated from interior C12A7:e⁻ via highly conductive Gr to the external Pd active species due to the work function gap between C12A7:e⁻ (ΦWF = 2.4 eV) and Pd (ΦWF = 5.1 eV).[39,40] The electron-rich Pd active sites enable the aryl halide activation and thereby reducing the apparent activation energy of Suzuki-coupling reaction by ca. 30%, so that the reaction could proceed under mild conditions. Impressively, Pd/Gr/C12A7:e⁻ showed no degradation in the catalytic activity even after impregnation of water, which demonstrates the chemical protection of Gr. These results demonstrate the effectiveness of combining an electride and traditional active metal, and reveal a simple and effective approach to improve catalytic activity and stability.

2. Results and discussion

The overall procedure for synthesis of the catalyst is illustrated in Fig. S1†. Nanometric Pd clusters were first deposited on the Gr surface using Na_2PdCl_4 as a Pd precursor and an ultraviolet (UV) light–induced reduction process. Both Gr and Pd/Gr could be dispersed uniformly in ethanol for a long time (Fig. S1† left), which suggests the thin nature of the Gr layers. The C12A7:e⁻ electride was fabricated by a conventional solid-phase reaction (see experimental section) and the surface area was around 1.0 $m^2 \cdot g^{-1}$. Subsequently, C12A7:e⁻ powder was mixed with fresh Pd/Gr in the solvent and stirred for 12 h. After vacuum-drying and annealing in an Ar atmosphere at 250 °C, Pd/Gr encapsulated C12A7:e⁻ (Pd/Gr/C12A7:e⁻) was obtained. It is noted that Pd/Gr/C12A7:e⁻ is easily collected because it settles to the bottom of the solvent (Fig. S1 † left), which indicates the formation of Pd/Gr and C12A7:e⁻ electride composite with increased material density. Fig. 2a and b show scanning electron microscopy (SEM) images of Pd/Gr/C12A7:e⁻ that reveal the C12A7:e⁻ particles were well encapsulated by Pd/Gr multi-layers and each element was uniformly distributed throughout the particles. The aberration-corrected high-angle annular dark-field (HAADF) scanning transmission electron microscopy (STEM) image in Fig. S2 † clearly shows that Pd clusters are uniformly dispersed on the Gr surface with a small average particle size of 1.5 nm.

When electronic conductive materials are in contact, a charge transfer is allowed to balance the chemical potentials of each material. For the Gr/C12A7:e⁻ heterostructure, an inorganic C12A7:e⁻ electride with a low work function of 2.4 eV could be regarded as an electron donor (Fig. S3†) for Gr with a higher work function of 5.0 eV, resulting in an electron transfer from C12A7:e⁻ to Gr (Fig. 1c),[39,40] which could be confirmed by Raman spectroscopy (Fig. 1d). In Raman spectra, the invariant D-band of Gr with and without C12A7:e⁻ suggests a physical interaction between C12A7:e⁻ and Gr. Comparatively, a blue-shift of G-band was appeared after the addition of C12A7:e⁻ electride. With reference to the results on carrier-injected carbon nanotubes,[41,42] this blue-shift should be ascribed to the lattice distortion of Gr evoked by the accepted electrons from C12A7:e⁻ and the Fermi level shift induced by electron-phonon coupling. Moreover, the C1s peak of X-ray photoelectron spectroscopy (XPS) of Pd/Gr/C12A7:e⁻ and Pd/Gr further show that the addition of C12A7:e⁻ up-shifted the binding energies of sp^3-hybridized carbon atoms, such as C=O, COOH and CO_3^{2-} over Gr layers, which means that electron transfer is mainly performed on the defect sites as well as functional groups of Gr (Fig. S4† and Table S1†). While C=C peak remains unchanged indicated no chemisorption process and modification of the graphitic structure. In combination with Raman shift, up-shifted C1s peaks in XPS spectra, it is reasonably to conclude that the electrons can be effectively transferred to Gr surface.

Given that Gr (ΦWF = 5.0 eV) and Pd (ΦWF = 5.1 eV) exhibit comparable work functions, the electron could be easily flowed between Gr and loaded Pd cluster. Negatively charged Pd species are thus realized, which was confirmed by X-ray absorption near-edge structure (XANES) measurement. The absorption edge for Pd species in Pd/Gr/C12A7:e⁻ was located at a lower energy relative to that of Pd foil (Fig. 1e), implying negatively charged Pd species. However, no energy shift was detected for Pd in Pd/Gr without the presence of C12A7:e⁻ electride. It is noted that Pd on C12A7:e⁻ was also in metallic form, which could be ascribed to the uneven charge distribution at large Pd particles on C12A7:e⁻ without the dispersion of Gr (Fig. S5†). As the surface reaction of the catalytic process, we then investigated the surface properties of the catalyst by using

This journal is © The Royal Society of Chemistry 20xx

Please do not adjust margins

XPS. Compared with the zero valence state of Pd (335.1 eV), the obvious lower energy shift of Pd 3d XPS peaks in Pd/Gr/C12A7:e⁻ implies electron-rich Pd species (334.7 eV) (Fig. 1f). These observations combined with the XANES analysis results indicate the key role of the C12A7:e⁻ electride as an electron donor in the modification of the electron density of the highly dispersed Pd clusters on Gr.

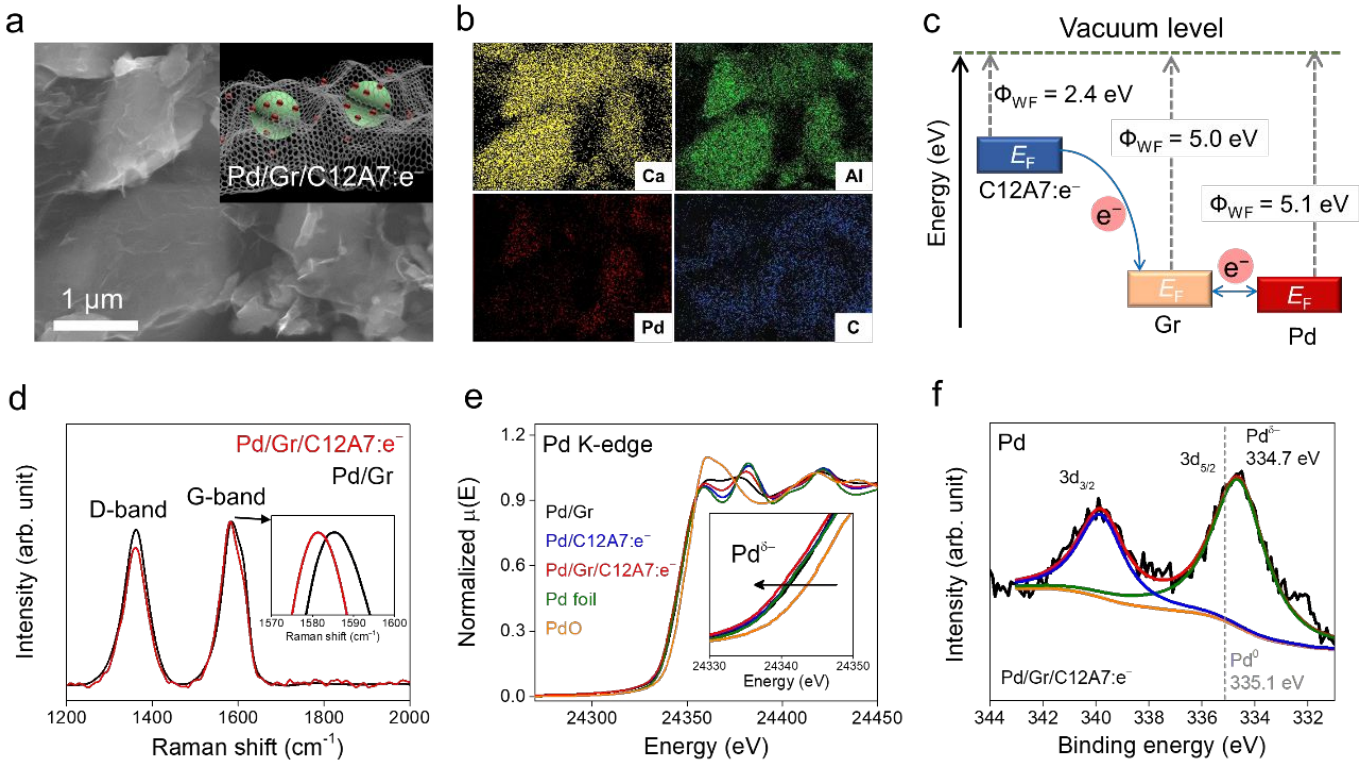

Fig. 1 Representative (a) SEM image and (b) corresponding elemental mapping of the Pd/Gr/C12A7:e⁻ composite catalyst. Inset (a): Schematic illustration of the structure of Pd/Gr/C12A7:e⁻. (c) Comparison of the Fermi level in the C12A7:e⁻ electride, Gr and Pd metal. Blue arrows indicate the direction of electron transfer from C12A7:e⁻ to Gr and Pd metal. (d) Raman spectra of Pd/Gr/C12A7:e⁻ and Pd/Gr respectively. The G-mode shift is magnified in the inset. (e) Pd K-edge XANES spectra of Pd in Pd/Gr/C12A7:e⁻. The data of Pd/Gr, Pd/C12A7:e⁻, Pd foil and PdO are also shown as references, which indicate the negatively charged Pd state in Pd/Gr/C12A7:e⁻. The Pd K-edge shift is magnified in the inset. (f) XPS spectra of Pd 3d in Pd/Gr/C12A7:e⁻. The grey dashed line represents the binding energy of the reference Pd metal with zero valence state.

We initially tested the possibility of using the negatively charged Pd active sites of the electride composite material in organic catalysis to promote Suzuki coupling of iodobenzene with phenylboronic acid as a model reaction. In Fig. 2a, Pd/Gr/C12A7:e⁻ showed high catalytic performance with a reaction rate of 60.0 mmol·g^{-1}·h^{-1} at room temperature, and its turnover frequencies (TOFs) value was estimated to be 1413.3h^{-1} based on the total amount of Pd, which is orders of magnitude larger than the Pd/Gr (5wt%Pd, 42.4h^{-1}), Pd/C12A7:e⁻ (1wt % Pd, 71.0 h^{-1}) and Pd/C12A7:O^{2-} (1wt % Pd, 43.5 h^{-1}) reference catalysts (Fig. 2a, Table S2†). Impressively, in terms of TOFs, Pd/Gr/C12A7:e⁻ even outperforms our previously reported negatively charge Pd catalysts (Pd/ZrC, $ZrPd_3$ and Y_3Pd_2) as well as other benchmarked commercial heterogeneous Pd catalysts (Lindlar catalyst from TCI, 5 wt% Pd; Pd/Al_2O_3 from Sigma-Aldrich, 5 wt% Pd; Pd/C from Sigma-Aldrich, 10 wt% Pd) 20-fold under the same reaction conditions (Table S3†). The lower reaction rates of Pd/C12A7:e⁻ (1wt % Pd) and Pd/C12A7:O^{2-} (1wt % Pd) is ascribed to the limited number of exposed active sites due to the large Pd particle size (Fig. S5 †, S6†). It is noted that the activity of Pd/C12A7:e⁻ (0.2wt % Pd, 1335.6 h^{-1}) is comparable to that of Pd/Gr/C12A7:e⁻ when the Pd particle size reduced (Fig. S7 †, Table S2 †), indicating an electron donation effect on nanosized Pd particles by C12A7:e⁻, which could also be confirmed by the same energy location of Pd 3d XPS spectra (Fig. S7b†). Also, with a similar Pd particle size (Fig. S8 †), the lower activity of the Pd/Gr sample is mainly attributed to the absence of C12A7:e⁻.

In addition to the high catalytic performance for the Suzuki coupling reactions, the stable recyclability of the Pd/Gr/C12A7:e⁻ catalyst should also be noted. Pd/Gr/C12A7:e⁻ catalyst can be recycled at least 8 times under both low (Fig. 2b) and high conversion (Fig. S9 †) levels. After the reaction, the crystal structure remained largely unchanged (Fig. S10 †). HAADF-STEM observation clearly revealed that the Pd particle size and morphology remained unchanged after recycling (Fig. S11†). XPS measurements showed that the Pd species remained in a negatively charged state, i.e., the surface electronic structure is highly stable (Fig. 2d). The hot filtration experiment indicated that the reaction only proceeds in the presence of Pd/Gr/C12A7:e⁻, and no more coupling products could be produced after removal of the Pd/Gr/C12A7:e⁻ catalyst (Fig. S12

Please do not adjust margins

†). Inductively coupled plasma atomic emission spectroscopy (ICP-AES) measurements also showed that the Pd species in the filtrate was below the detection limit (0.007 ppm). These results for the used Pd/Gr/C12A7:e⁻ catalyst demonstrated the robustness of the Pd active sites and confirmed the excellent stability of this catalyst.

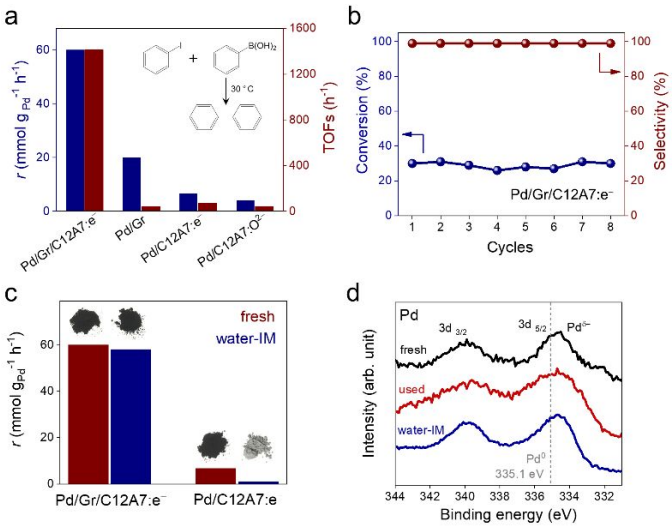

Fig. 2 (a) Reaction rates and TOFs for the coupling of iodobenzene and phenylboronic acid over Pd/Gr/C12A7:e⁻, Pd/Gr, Pd/C12A7:e⁻ and Pd/C12A7:O^{2-} catalysts. (b) Recycling experiment for the coupling reaction over Pd/Gr/C12A7:e⁻. (c) Reaction rates over fresh and water impregnated (IM) Pd/Gr/C12A7:e⁻ and Pd/C12A7:e⁻ for the coupling of iodobenzene and phenylboronic acid with photographs of the corresponding catalysts powders. (d) XPS spectra of Pd 3d over fresh, used and water IM Pd/Gr/C12A7:e⁻ catalysts. The grey dashed line represents the binding energy of the reference Pd metal with zero valence state.

Moisture sensitivity is one of the most serious obstacles to the practical application of C12A7:e⁻ electride, which always undergone transformation from C12A7:e⁻ to Ca and Al hydrates with the release of the anionic electron that significantly reduces its carrier density.[43] However, Pd/Gr/C12A7:e⁻ was found to be robust against water. A Suzuki coupling reaction using water impregnated Pd/Gr/C12A7:e⁻ powder as a catalyst was conducted without change to any other conditions. The obtained coupling rate was almost identical to that of the fresh catalyst and the color of the samples did not change (Fig. 2c). Decomposition of the catalyst, such as by the generation of Ca and Al hydrates, was not identified from X-ray diffraction (XRD) measurements after the impregnation in water (Fig. S10 †). Based on XPS measurements, the partially negatively charged Pd was not affected by the water impregnation, which demonstrates the robustness of the Pd/Gr/C12A7:e⁻ catalyst (Fig. 2d). In contrast, the catalytic activity of the Pd/C12A7:e⁻ catalyst was obviously degraded after impregnation in water and the colour of the sample changed from black to light grey, associated with the transformation to the related Ca and Al hydrates (Fig. 2c). This degradation can be attributed to the absence of the protective layer of Gr, which results in the progressive release of the anionic electrons from C12A7:e⁻.

To further investigate the electron donation effect of C12A7:e⁻, the controlled electron concentration (N_e) of C12A7:e⁻ was investigated. C12A7:e⁻ with different N_e were obtained by the treatment with Ti metal at different temperatures (Fig. 3).Fig. 3a shows the UV-vis absorption spectra for the synthesized powders of C12A7:e⁻ or C12A7:O^{2-} with various N_e. There is no adsorption peak of the C12A7:O^{2-} sample (orange line) in the visible region, and the corresponding 3.5 eV absorption edge is attributed to the excitation between the energy level of encaged O^{2-} ions and the cage conduction band (CCB).[44] While, a broad absorption peak at around 2.3~2.7 eV (2.3 eV, 2.5 eV and 2.7 eV for green, blue and red lines respectively) appeared in C12A7:e⁻ which can be attributed to an intra-cage transition of electrons confined in the cages. The other absorption peak below 2 eV is ascribed to an inter-cage transition as charge transfer occurs from an electron-trapped cage to a neighboring vacant cage.[45] Therefore, it can be deduced that O^{2-} ions in the cages of C12A7:O^{2-} are substituted by electrons and thus forming C12A7:e⁻. Refer to our previous studies, the adsorption peak position (E_{sp}) and electron concentration (N_e) are related to the following equation: $N_e = [-(E_{sp} - E_{sp}°)/0.199]^{0.782}$, and one typical case is that $E_{sp}° = 2.83$ eV represents $N_e \approx 1.0 \times 10^{18}$ cm^{-3}.[46] Thus, the electron concentrations of the above C12A7:e⁻ samples can be calculated to be 1.2×10^{20}, 1.1×10^{21}, and 2.2×10^{21} cm^{-3} respectively (Fig. 3b). Accordingly, the sample color was changed from white by green to black with increased N_e (Fig. 3b).

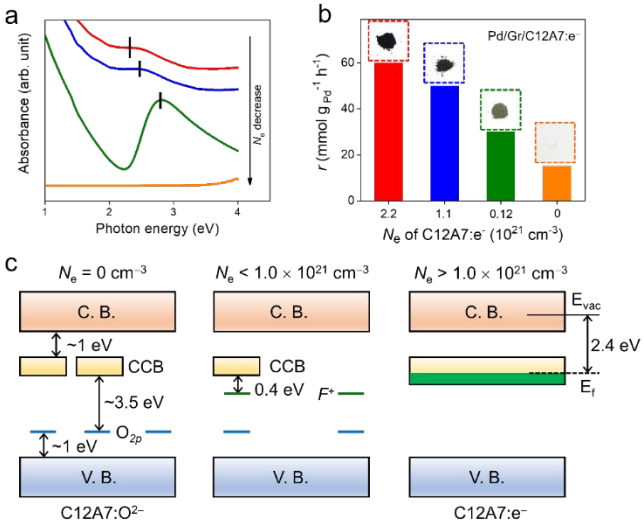

Fig. 3 (a) The UV-vis absorption spectra for the synthesized powders of C12A7:e⁻ or C12A7:O^{2-} with various electron concentration (N_e). The electron concentrations corresponding to the red, blue, green and orange lines are 2.2×10^{21}, 1.1×10^{21}, 1.2×10^{20} and 0 cm^{-3}, respectively. (b) Reaction rates over the Pd/Gr/C12A7:e⁻ catalyst as a function of the electron concentration of C12A7:e⁻, and corresponding photographs of the synthesized powders of C12A7:e⁻ with various N_e. (c) Scheme of the electronic structures of C12A7:O^{2-} and C12A7:e⁻ with various N_e.

Fig. 3c shows the electronic structures of C12A7:e⁻ or C12A7:O^{2-} with various range of N_e. For C12A7:O^{2-} with N_e = 0 cm^{-3}, the 2*p* orbitals of the framework O^{2-} ions and 4s orbitals of the framework Ca^{2+} ions contributed to the valence band (VB) and conduction band (CB) respectively. In contrast to framework O^{2-} ions, the energy level of the encaged O^{2-} ions located slightly above the top of VB of the cage framework. While, the electron tunneling among the three-dimensionally

This journal is © The Royal Society of Chemistry 20xx

Please do not adjust margins

connected cages enable the formation of the CCB, which is located at ~1.0 eV below the bottom of CB.[47] In the case of $N_e < 1.0 \times 10^{21}$ cm^{-3}, the cage encaged electrons in with low density formed an F^+-like center and energy level is located 0.4 eV below the CCB. When the N_e is higher than 1.0×10^{21} cm^{-3}, the cage trapped electrons occupy the CCB, raising the Fermi level of C12A7:e$^-$ to 0.5 eV above the CCB minimum. Therefore, an intrinsic low work function property was realized over such unique electron occupied CCB electronic structure. The high electron concentration leading to a low work function property enables a high electron donation power for C12A7:e$^-$. The catalytic activity of Pd/Gr/C12A7:e$^-$ provides information on the critical electron concentration (N_e) of C12A7:e$^-$ as a support. Impressively, the reaction rates were observed to be increased monotonically with the N_e of C12A7:e$^-$ (Fig. 3b). This observation suggests that the catalytic activity of this reaction is directly proportional to the electron donation ability of the support. Accordingly, the measured apparent activation energy (E_a) decreases from 83.0 kJ·mol^{-1} to 58.7 kJ·mol^{-1} with increasing N_e (Fig. S13 †), which should be related to the electron transfer from C12A7:e$^-$ via surface Pd active sites to aryl halide substrates.

Table 1 Suzuki cross-coupling reactions of various aryl halides with arylboronic acids over the Pd/Gr/C12A7:e$^-$ catalyst.

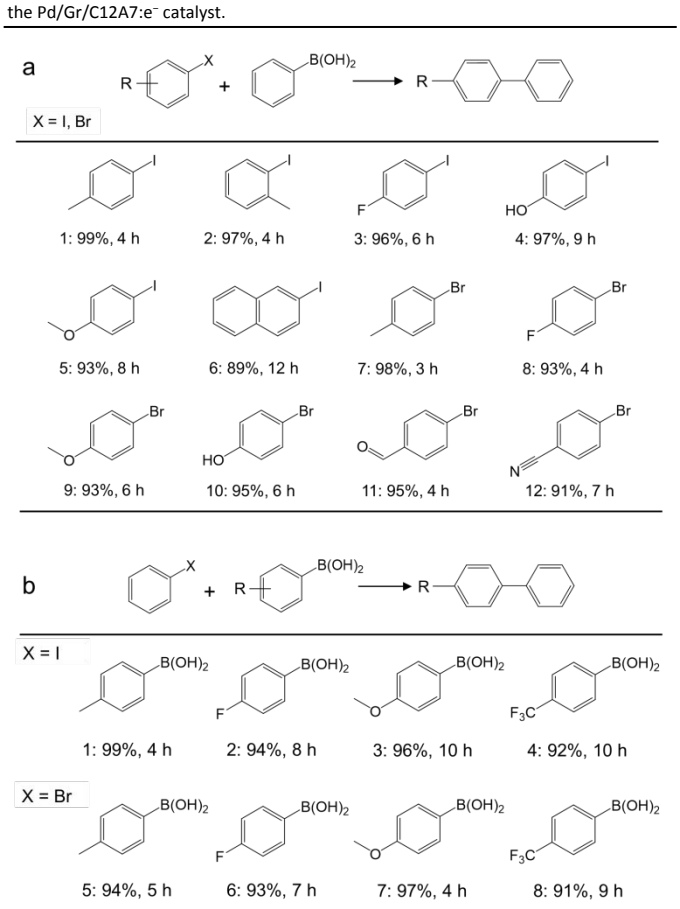

Reaction conditions: Pd (0.47 mol% relative to organohalide), 0.5 mmol organohalide, 0.8 mmol arylboronic acid, 1.5 mmol K_2CO_3, 5 mL ethanol, iodides 30 ºC, bromides 60 ºC. The yields given below the structure were determined using GC and GC−MS.

Application of the catalyst was then extended to various aryl halides and boronic acids to verify the general activity of the Pd/Gr/C12A7:e$^-$ catalyst towards Suzuki coupling reactions. Table 1a shows that all of the tested aryl halides with a range of functional groups could be converted to the corresponding coupled products in high yields, regardless of whether the functional groups were electron-donating or electron-withdrawing. Next, different types of boronic acids were further exploited as coupling partners (Table 1b). The results confirmed the general applicability of the Pd/Gr/C12A7:e$^-$ catalyst with high selectivity and functional group tolerance. In addition, the coupling reaction of chlorobenzene with boronic acids was also investigated (Table S4†), the activity for producing diphenyl was poor which should be ascribed the much higher bonding energy of C−Cl (346 kJ mol^{-1}) than those of C−Br (290 kJ mol^{-1}) and C−I (228 kJ mol^{-1}).[48]

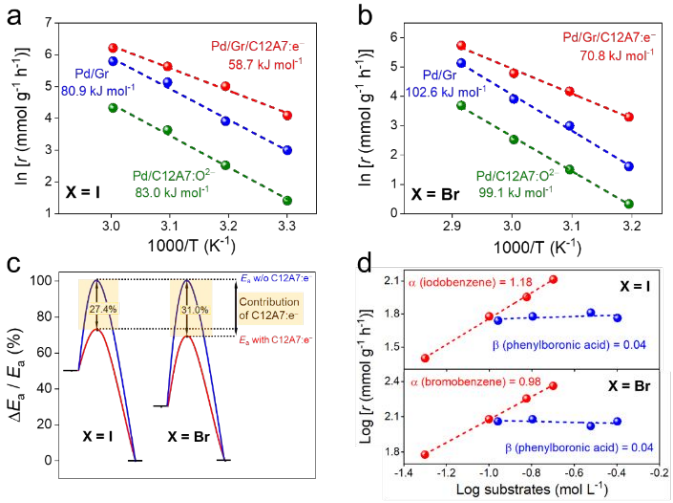

Fig. 4 Arrhenius plots of Suzuki cross-coupling reactions performed using (a) iodobenzene and (b) bromobenzene as substrates over Pd/Gr/C12A7:e$^-$ and Pd/Gr catalysts. Reaction conditions: Pd (0.47 mol% relative to organohalide), 0.5 mmol organohalide, 0.8 mmol arylboronic acid, 1.5 mmol K_2CO_3 and 5 mL solvent. (c) Apparent activation energies (E_a) calculated for the Suzuki cross-coupling reactions over catalysts with and without C12A7:e$^-$. (d) Reaction rate dependence on the organohalide and arylboronic acid concentration over the Pd/Gr/C12A7:e$^-$ catalyst.

Next, Arrhenius plots were plotted to investigate the apparent activation energies (E_a) of the Suzuki coupling over the Pd/Gr/C12A7:e$^-$, Pd/Gr and Pd/C12A7:O^{2-} catalysts. The E_a of Pd/Gr/C12A7:e$^-$ was estimated to be 58.7 kJ mol−1 of the coupling reaction of iodobenzene and phenylboronic acid (Fig. 4a), which shows a ca. 27.4% and 29.3% reduction compare with those of Pd/Gr (80.9 kJ·mol^{-1}) and Pd/C12A7:O^{2-} (83.0 kJ·mol^{-1}) respectively (Fig. 4c). Meanwhile, the E_a follows the same trend with the iodobenzene replaced by bromobenzene (Fig. 4b), in which the calculated E_a of Pd/Gr/C12A7:e$^-$ (70.8 kJ·mol^{-1}) is ca. 31.0% and 28.6% less than that of Pd/Gr (102.6 kJ·mol^{-1}) and Pd/C12A7:O^{2-} (99.1 kJ·mol^{-1}) respectively (Fig. 4c). These results suggest that the Suzuki coupling reaction is promoted in the presence of C12A7:e$^-$. Kinetic reaction orders were estimated by changing the concentration of aryl halides and phenylboronic acid over Pd/Gr/C12A7:e$^-$. Fig. 4d shows that both reaction rates are sensitive to the concentration of aryl halides but independent of the phenylboronic acid. These results imply that the activation of aryl halides controlled the

Please do not adjust margins

overall reaction process over Pd/Gr/C12A7:e⁻, which is well accepted for both homogeneous and heterogeneous Pd based catalysts in Suzuki coupling reactions, i.e., the oxidative addition of the aryl halide is the rate-determining step for the catalytic cycle.[49-52] From this kinetic analysis, the smaller E_as and reaction orders reveal that the enhanced activity of Pd/Gr/C12A7:e⁻ over that for the Pd/Gr catalyst exclusively originates from the promoted activation of the aryl halides.

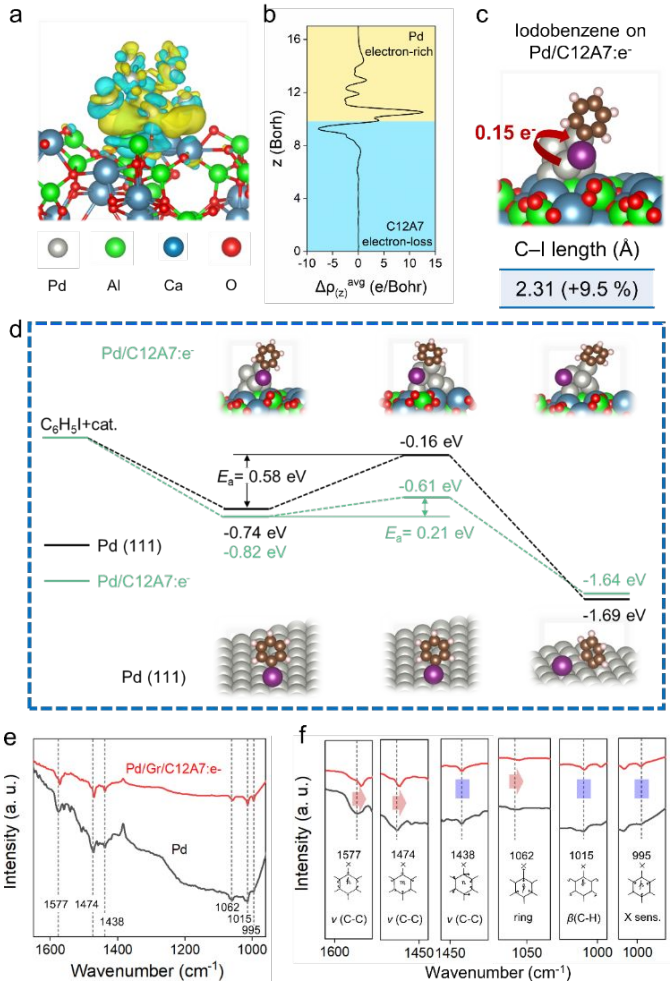

Fig. 5 Depictions of the electronic interaction between catalysts and aryl halide. (a) 3D electron density isosurface map and (b) planar-averaged electron density difference Δρ (z) of Pd/C12A7:e⁻.The yellow and cyan areas indicate electron accumulation and depletion, respectively. (c) Adsorption of iodobenzene on Pd/C12A7:e⁻. A view of the system from the size and C–I bond lengths are shown at the bottom. (d) Energy profiles from DFT studies of the activation of iodobenzene on Pd/C12A7:e⁻ and Pd (111) surfaces. (e) DRIFTS spectra for the adsorption of iodobenzene onto Pd and Pd/Gr/C12A7:e⁻, respectively. (f) Enlarged DRIFTS spectra emphasizes the redshift of the C-I bond related vibration on Pd/Gr/C12A7:e⁻.

To further understand the activation behaviours of aryl halides, DFT calculations and in-situ diffuse reflectance infrared Fourier transform spectroscopy (DRIFTS) spectra were also performed. As illustrated in Fig. 5a and 5b, obvious electron deficient and rich regions are constructed at the interface between C12A7:e⁻ and Pd. The elevated electron density of Pd sites enable the electron transfer (0.15e⁻) to the adsorbed iodobenzene substrate, thereby weakening the C-I bond with 9.5% elongation (Fig. 5c). Here, the reaction barriers for the oxidative addition of the aryl halide was also calculated over Pd/C12A7:e⁻ and Pd (111). The activation process of iodobenzene molecule proceeds with an energy barrier of 0.21eV on Pd/C12A7:e⁻, much lower than that of 0.58 eV on Pd (111) (Fig. 5d). The tendency of the suppressed activation energy agrees well with the experimental observations, further suggesting the activation step of aryl halide on Pd/C12A7:e⁻ is remarkably enhanced.

Next, the adsorption behaviour of iodobenzene is experimentally evaluated using DRIFT spectroscopy (Fig. 5e). For Pd (111), the black line shows bands in the range of 1400–1600 cm^{-1}, associated with C–C stretching in aromatic vibration (νC–C).[53] In the low frequency region, the IR vibrational bands of halogen-sensitive vibration (995 cm^{-1}), out-of-plane C–H deformation (β(C–H): 1015 cm^{-1}), trigonal ring breathing (1062 cm^{-1}) can be observed. Notably, if the catalyst changed to Pd/Gr/C12A7:e⁻, the IR vibrational peaks of 1577 and 1474 cm^{-1} associated with the admixture of C–I deformation show a significant redshift compared to pure Pd case (Fig. 5f). While, a similar redshift was also detected for the C–I stretching vibration (1062 cm^{-1}, Fig. 5f). The both redshift phenomenon of the C–I bond related vibration indicated the carbon halogen bond weakening process. These results are consistent with the DFT calculation results, in which the low work function C12A7:e⁻ electride generally acts as an electron-donating ligand and improves the electron donation to the antibonding orbitals of the aryl halides through the surface Pd active sites, which accounts for the carbon halogen bond weakening, the rate-determining step of the reaction. The results of the kinetic analysis suggest the importance of the electronic effect between C12A7:e⁻ and the highly dispersed active Pd species in terms of electron density modification, which results in the significant enhancement of the catalytic activity of Pd active sites towards the cross-coupling reaction.

Table 2 Performance of Pd/Gr/C12A7:e⁻ for various cross-coupling reactions.

Entry	Aryl Halides	Coupling Partner	Product	Time (h)	Yield (%)
[a]1				12	93
[a]2		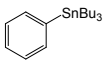	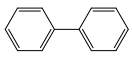	18	91
[b]3		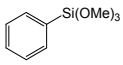	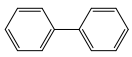	24	82
[b]4			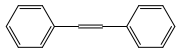	24	88

Reaction conditions: Pd (0.47 mol% relative to organohalide); 0.5 mmol iodobenzene, 0.8 mmol coupling Partner, 1.5 mmol K_2CO_3, [a]5 mL ethanol, 60 °C, [b]5 mL DMF, 120 °C. The yields given below the structure were determined using GC and GC–MS.

Owing to high activity of the activation of aryl halides over Pd/Gr/C12A7:e⁻, we became interested in testing the catalyst

This journal is © The Royal Society of Chemistry 20xx

Please do not adjust margins

for various C–C couplings such as Sonogashira, Stille, Hiyama and Heck coupling reactions. As shown in Table 2, each of the tested iodobenzene and coupling partners, such as phenylacetylene, tributylphenylstannane, phenylethylene, trimethoxyphenylsilane, could be converted to the corresponding coupled products in a high yield. The results confirmed the versatile applicability of the Pd/Gr/C12A7:e^- catalyst for various C–C cross coupling reactions.

3. Conclusions

In summary, we successfully designed and prepared an electride composite material Pd/Gr/C12A7:e^-, in which nanometric Pd clusters are dispersed on a Gr support with encapsulated C12A7:e^- electride. The intermediate Gr layer not only serves as an excellent electron transport medium to promote electron transfer from the internal C12A7:e^- electride to external Pd active sites, but also as a protective layer for the C12A7:e^- electride against water. The obtained Pd/Gr/C12A7:e^- catalyst hosts both highly dispersed and partially negatively charged Pd active sites, allowing the cross-coupling reaction to proceed with reduced activation energies. Mechanistic studies demonstrated that the strong electron donation ability of the C12A7:e^- electride enabled negatively charged Pd sites through a multistep electron transfer process to promote the activation of aryl halides, which is the rate-determining step for the investigated cross-coupling reactions. Pd/Gr/C12A7:e^- could also be easily separated and recycled for more than eight cycles without significant loss of activity. The present efficient catalyst can further trigger various carbon-carbon cross-coupling reactions such as Sonogashira, Stille, Hiyama and Heck coupling with high activities.

4. Experimental section

4.1 Sample preparation

The Gr powder used in this study was purchased from Sigma Aldrich, Ltd. (USA). Prior to deposition, the Gr powder was pre-treated at 400 °C for 5 h in vacuum (ca. 1×10^{-4} Pa) to remove water and oxygen adsorbed on the surface. It is noted that the thickness of the commercial Gr was less than three layers according to the instruction of the product. The treated Gr powder was dispersed in a solution of Na_2PdCl_4 in ethanol and continuously stirred under UV irradiation (Xe lamp parallel light source system). After UV treatment for 30 min, the sample was centrifuged, washed three times with ethanol and water, and then dried in a vacuum oven to obtain Pd/Gr. C12A7:O^{2-} (C12A7) powders were synthesized by a conventional solid-state reaction of $CaCO_3$ and α-Al_2O_3 with a molar ratio of 12:7 at 1300 °C for 20 h in an air atmosphere. Pd loading was conducted using the same method as was used for Gr. C12A7:e^- electride was prepared by the reaction of C12A7:O^{2-}, $CaO\cdot Al_2O_3$ (CA) and Ti metal at 900~1100 °C. Typically, the C12A7:O^{2-} powder was sealed in a quartz tube with Ti metal under a vacuum of ~ 10^{-3} torr. Then the sealed tube was thermally annealed at temperatures of 900~1100 °C for 24–72 hrs. Adjusting the temperature and duration of the Ti-treatment replaces all or a part of the free oxygen ions with electrons by the reaction, Ti (surface) + xO^{2-} (cage) → TiO_x (surface) + $2xe^-$ (cage), which forms electron-doped C12A7. The C12A7:e^- samples with various electron concentrations of 1.2×10^{20}, 1.1×10^{21} and 2.2×10^{21} cm^{-3} are obtained by the heat treatment of C12A7:O^{2-} under the temperature of 900, 1000, 1100 °C, respectively. Then the obtained C12A7:e^- powder was mixed with fresh Pd/Gr (weight ratio of C12A7:e^- and Pd/Gr of 10:1) and stirred overnight in super dry ethanol. After drying in a vacuum and annealing in an Ar atmosphere at 250 °C for 6 h, Pd/Gr encapsulated C12A7:e^- (Pd/Gr/C12A7:e^-) was obtained.

4.2 Procedure for catalytic reactions

The cross-coupling reactions were carried out in a 25 mL stainless steel autoclave equipped with a magnetic stirrer. In a typical reaction, 0.5 mmol aryl halides, 0.8 mmol coupling partners (arylboronic acids, phenylacetylene, tributylphenylstannane, trimethoxyphenylsilane, phenylethylene), 1.5 mmol K_2CO_3, and Pd (0.47 mol% relative to aryl halides) catalyst were mixed together in 5 mL solvent. The autoclave was then flushed three times with Ar, and the reaction was performed at the temperature range of 30 to 70 °C. The products were analyzed by gas chromatography (GC) and gas chromatography-mass spectrometry (GC-MS) was used to further confirm the coupling product. The TOF was calculated according to the reaction rate at a low conversion level derived from the total number of Pd atoms used in the catalyst.

To check whether the coupling reaction over Pd/Gr/C12A7:e^- catalyst is a heterogeneous reaction, the catalyst was removed from the reaction mixture by a hot filtration after 1 h of reaction, and the filtrate proceed under the same reaction condition. For the stability test, each coupling reaction of aryl halides and phenylboronic acid was conducted at the same conditions. After the finish of each coupling reaction, the catalyst powder was separated via centrifugation followed by washing three times with ethanol and water to remove the organic and inorganic residues. After that, the catalyst powder was allowed to dry in a vacuum at room temperature, weighed, and reused in the next run. For the moisture resistant test, Pd/Gr/C12A7:e^- powder was impregnated in water for 1 h at room temperature. The catalyst powder was then separated via centrifugation followed by the removal of water and drying in a vacuum overnight.

4.3 Sample characterization

The crystal structure was analyzed using XRD (D8 Advance, Bruker) with monochromate Cu Kα radiation (λ = 0.15418 nm). XPS (ESCA-3200, Shimadzu) measurements were performed using Mg Kα radiation at $<10^{-6}$ Pa (8 kV bias voltage applied to the X-ray source). The morphology of the sample was evaluated by aberration-corrected HAADF-STEM (JEM ARM-200F, JEOL) at 200 kV. Before the measurement, the powder sample was dispersed in super dry ethanol and dropwise added onto a holey carbon film with copper mesh. For scanning electron

Please do not adjust margins

microscopy (SEM) test, the sample powders were also dispersed onto an Al-stub and examined in SE and backscatter modes using JSM-7600F, JEOL equipped with an energy dispersive X-ray spectrometer (EDX). The diameters of Pd particle were estimated by counting the sizes of more than 100 particles for each sample. X-ray absorption fine structure (XAFS) measurements were carried out on the BL-12C beamline. To obtain the monochromatized X-ray beam, a Si(111) double-crystal monochromator was used, and the corresponding spectra were recorded in transmission mode by diluting samples in BN powder. The Pd content was determined using ICP-AES (ICPS-8100, Shimadzu). To evaluate the Brunauer-Emmett-Teller (BET) surface area, nitrogen sorption measurements were conducted by using an adsorption analyzer (BELSORP-mini II, BEL, Japan). Prior to measurements, the catalysts were degassed in a vacuum at 150 °C for 12 h.

4.4 DFT calculations

All DFT calculations were conducted using the Vienna ab initio simulation package (VASP).[54,55] The generalized gradient approximation method with the Perdew–Burke– Ernzerhof (PBE)[56] exchange–correlation functional was used to manage the electron exchange and related energy, the core electrons were described using the projector augmented wave (PAW) method.[57,58] The plane wave basis kinetic energy with a cut-off value of 450 eV was employed to describe the valence electrons. A mesh of 2 × 2 × 1 was used for the k-point sampling obtained from the Gamma center. Meanwhile, in the case of system, the unit cell was 11.79 × 11.87 × 25 Å^3, the thickness of the vacuum layer was 20 Å. All models were fully optimized until the energy and forces are converged to 1 × 10^{-5} eV and 0.0257 eV Å^{-1}, respectively. For transition state (TS) calculation, the parameters of CI-NEB[59,60] are kept the same as the structure relaxation. The calculations of the intermediates binding energy were conducted following the equation:

$\Delta E_{*x} = E_{sys} – E_{slab} - E_x$.

While E_{sys}, E_{slab} and E_x is the calculated energy of slab adsorbed intermediate model, slab model and intermediated model, respectively.

Author Contributions

J.-S. C. proposed the idea behind the research and T.-N.Y. supervised the project. B. D., M.X., Y.L., J.L., J. Z., L. F., X.-H.L. and M.K. performed the synthesis, characterization and catalytic measurements. Z.L. and S.-W.P. conducted the model construction and DFT calculations. M.S. conducted STEM measurements. T.-N.Y., M.K., H.H. and J.-S.C. co-wrote the paper. All authors discussed the results and commented on the manuscript.

Conflicts of interest

The authors declare no competing financial interest.

Acknowledgements

This work was supported by the National Natural Science Foundation of China (22105122, 22275121), the Science and Technology Commission of Shanghai Municipality (21PJ1407400), Shanghai Municipal Science and Technology Major Project and the Open Foundation Commission of Shaoxing Research Institute of Renewable Energy and Molecular Engineering (JDSX2022038). A part of this work was also supported by Element Strategy Initiative to Form Core Research Center (Grant Number JPMXP0112101001) of the Ministry of Education, Culture, Sports, Science and Technology (MEXT) of Japan, Kakenhi Grants-in-Aid (JP17H06153, JP22H00272) from the Japan Society for the Promotion of Science (JSPS) and JST FOREST Program (JPMJFR203A).

Notes and references

1 A. Suzuki, *Angew. Chem. Int. Ed*, 2011, **50**, 6722–6737.
2 N. Miyaura and A. Suzuki, *Chem. Rev,* 1995, **95**, 2457–2483.
3 C. C. C. J. Seechurn, M. O. Kitching, J. Colacot and T. V. Snieckus, *Angew. Chem. Int. Ed,* 2012, **51**, 5062–5085.
4 B. W. Glasspoole and C. M. Crudden, *Nat. Chem.* 2011, **3**, 912–913.
5 G. C. Fu, *Acc. Chem. Res.* 2008, **41**, 1555−1564.
6 S. L. Buchwald, *Acc. Chem. Res.* 2008, **41**, 1461–1473.
7 L. Yin and J. Liebscher, *Chem. Rev.* 2007, **107**, 133–173.
8 Á. Molnár, *Chem. Rev.* 2011, **111**, 2251-2320.
9 A. F. Littke and G. C. Fu, *Angew. Chem. Int. Ed.* 2002, **41**, 4176–4211.
10 T. N. Ye, Y. F. Lu, Z. Xiao, J. Li, T. Nakao, H. Abe, Y. Niwa, M. Kitano, T. Tada and H. Hosono, *Nat. Commun.* 2019, **10**, 5653.
11 Y. F. Lu, T. N. Ye, S. W. Park, J. Li, M. Sasase, H. Abe, Y. Niwa, M. Kitano and H. Hosono, *ACS Catal.* 2020, **10**, 14366–14374.
12 B. Sun, L. Ning and H. C. Zeng, *J. Am. Chem. Soc.* 2020, **142**, 13823–13832.
13 G. M. Scheuermann, L. Rumi, P. Steurer, W. Bannwarth and R. Mulhaupt, *J. Am. Chem. Soc.* 2009, **131**, 8262–8270.
14 B. Yuan, Y. Pan, Y. Li, B. Yin and H. Jiang, *Angew. Chem. Int. Ed.* 2010, **49**, 4054–4058.
15 T. Noël, S. Kuhn, A. J. Musacchio, K. F. Jensen and S. L. Buchwald, *Angew. Chem. Int. Ed.* 2011, **50**, 5943–5946.
16 Ö. Metin, S. F. Ho, C. Alp, H. Can, M. N. Mankin, M. S. Gültekin, M. Chi and S. Sun, *Nano Res.* 2013, **6**, 10–18.
17 Y. Wu, D. Wang, P. Zhao, Z. Niu, Q. Peng and Y. Li, *Inorg. Chem.* 2011, **50**, 2046–2048.
18 T. N. Ye, J. Li, M. Kitano, M. Sasase and H. Hosono, *Chem. Sci.* 2016, **7**, 5969–5975.
19 X. H. Li, M. Baar, S. Blechert and M. Antonietti, *Sci. Rep.* 2013, **3**, 1743.
20 W. Ke, T. Cui, Q. Yu, M. Wang, L. Lv, H. Wang, Z. Jiang, X. H. Li and J. Chen, *Nano Res.* 2018, **11**, 874–881.
21 T. N. Ye, J. Li, M. Kitano and H. Hosono, *Green Chem.* 2017, **19**, 749–756.
22 Z. Chen, E. Vorobyeva, S. Mitche, E. Fako, M. A. Ortuño, N. López, S. M. Collins, P. A. Midgley, S. Richard, G. Vilé and J. Pérez-Ramírez, *Nat. Nanotech.* 2018, **13**, 702–707.
23 S. Lu, Y. Hu, S. Wan, R. McCaffrey, Y. Jin, H. Gu and W. Zhang, *J. Am. Chem. Soc.* 2017, **139**, 17082−17088.
24 H. Hosono and M. Kitano, *Chem. Rev.* 2021, **121**, 3121−3185.
25 S. Matsuishi, Y. Toda, M. Miyakawa, K. Hayashi, T. Kamiya, M. Hirano, I. Tanaka and H. Hosono, *Science* 2003, **301**, 626−629.
26 K. Lee, S. W. Kim, Y. Toda, S. Matsuishi and H. Hosono, *Nature* 2013, **494**, 336–340.

This journal is © The Royal Society of Chemistry 20xx

Please do not adjust margins

27 Y. F. Lu, J. Li, T. Tada, Y. Toda, S. Ueda, T. Yokoyama, M. Kitano and H. Hosono, *J. Am. Chem. Soc.* 2016, **138**, 3970−3973.
28 T. N. Ye, Y. F. Lu, J. Li, T. Nakao, H. S. Yang, T. Tada, M. Kitano and H. Hosono, *J. Am. Chem. Soc.* 2017, **139**, 17089–17097.
29 J. Z. Wu, Y. T. Gong, T. Inoshita, D. C. Fredrickson, J. J. Wang, Y. F. Lu, M. Kitano and H. Hosono, *Adv. Mater.* 2017, **29**, 1700924.
30 J. Z. Wu, J. Li, Y. T. Gong, M. Kitano, T. Inoshita and H. Hosono, *Angew. Chem., Int. Ed.* 2019, **58**, 825–829.
31 M. Kitano, Y. Inoue, Y. Yamazaki, F. Hayashi, S. Kanbara, S. Matsuishi, T. Yokoyama, S. W. Kim, M. Hara and H. Hosono, *Nat. Chem.* 2012, **4**, 934–940.
32 M. Kitano, S. Kanbara, Y. Inoue, N. Kuganathan, P. V. Sushko, T. Yokoyama, M. Hara and H. Hosono, *Nat. Commun.* 2015, **6**, 6731.
33 S. Kanbara, M. Kitano, Y. Inoue, T. Yokoyama, M. Hara and H. Hosono, *J. Am. Chem. Soc.* 2015, **137**, 14517–14524.
34 F. Hayashi, Y. Toda, Y. Kanie, M. Kitano, Y. Inoue, T. Yokoyama, M. Hara and H. Hosono, *Chem. Sci.* 2013, **4**, 3124–3130.
35 H. Buchammagari, Y. Toda, M. Hirano, H. Hosono, D. Takeuchi and K. Osakada, *Org. Lett.* 2007, **9**, 4287–4289.
36 S. M. Kim, H. S. Yoo, H. Hosono, J. W. Yang and S. W. Kim, *Sci. Rep.* 2015, **5**, 10366.
37 J. Bong, T. Lim, K. Seo, C. Kwon, J. H. Park, S. K. Kwak and S. Ju, *Sci. Rep.* 2015, **5**, 14321.
38 W. Wei, S. Yang, H. Zhou, I. Lieberwirth, X. Feng and K. Müllen, *Adv. Mater.* 2013, **25**, 2909–2914.
39 Y. Toda, H. Yanagi, E. Ikenaga, J. J. Kim, M. Kobata, S. Ueda, T. Kamiya, M. Hirano, K. Kobayashi and H. Hosono, *Adv. Mater.* 2007, **19**, 3564–3569.
40 J. M. Beebe, V. B. Engelkes, L. L. Miller and C. D. Frisbie, *J. Am. Chem. Soc.* 2002, **124**, 11268–11269.
41 Y. N. Gartstein, A. A. Zakhidov and R. H. Baughman, *Phys. Rev. Lett.* 2002, **89**, 045503.
42 M. M. Menamparambath, J. Park, H. Yoo, S. P. Patole, J. Yoo, S. W. Kim and S. Baik, *Nanoscale* 2014, **6**, 8844–8851.
43 Park, C. K. *Cem. Concr. Res.* 1998, **28**. 1357–1362.
44 K. Hayashi, P. V. Sushko, D. M. Ramo, A. L. Shluger, S. Watauchi, I. Tanaka, S. Matsuishi, M. Hirano and H. Hosono, *J. Phys. Chem. B* 2007, **111**, 1946–1956.
45 S. Matsuishi, S. W. Kim, T. Kamiya, M. Hirano and H. Hosono, *J. Phys. Chem. C* 2008, **112**, 4753–4760.
46 S. Matsuishi, T. Nomura, M. Hirano, K. Kodama, S. Shamoto and H. Hosono, *Chem. Mater.* 2009, **21**, 2589–2591.
47 P. V. Sushko, A. L. Shluger, M. Hirano and H. Hosono, *J. Am. Chem. Soc.* 2007, **129**, 942–951.
48 A. Leyva-Perez, J. Oliver-Meseguer, P. Rubio-Marqués and A. Corma, Angew. *Chem. Int. Ed.* 2013, **52**, 11554–11559.
49 F. Wang, C. Li, H. Chen, R. Jiang, L. Sun, Q. Li, J. Wang, J. C. Yu and C. Yan, *J. Am. Chem. Soc.* 2013, **135**, 5588–5601.
50 X. Zhang, Z. Sun, B. Wang, Y. Tang, L. Nguyen, Y. Li and F. F. Tao, *J. Am. Chem. Soc.* 2018, **140**, 954−962.
51 S. Sarina, H. Zhu, E. Jaatinen, Q. Xiao, H. Liu, J. Jia, C. Chen and J. Zhao, *J. Am. Chem. Soc.* 2013, **135**, 5793−5801.
52 Q. Xiao, S. Sarina, A. Bo, J. Jia, H. Liu, D. P. Arnold, Y. Huang, H. Wu and H. Zhu, *ACS Catal.* 2014, **4**, 1725–1734.
53 D. H. Whiffen, *J. Chem. Soc.* 1956, **273**, 1350−1356.
54 G. Kresse and J. Hafner, *Phys. Rev. B: Condens. Matter.* 1993, **47**, 558–561.
55 G. Kresse and J. Furthmüller, *Comput. Mater. Sci.* 1996, **6**, 15–50.
56 G. Kresse and D. Joubert, *Phys. Rev. B* 1999, **59**, 1758–1775.
57 P. E. Blöchl, *Phys. Rev. B* 1994, **50**, 17953–17979.
58 J. P. Perdew, K. Burke and M. Ernzerhof, *Phys. Rev. Lett.* 1996, **77**, 3865–3868.
59 G. Henkelman, B. P. Uberuaga and H. Jónsson, *J. Chem. Phys.* 2000, **128**, 9901–9904.
60 G. Henkelman and H. Jónsson, *J. Chem. Phys.* 2000, **113**, 9978–9985.

This journal is © The Royal Society of Chemistry 20xx

Please do not adjust margins